

Gamma Ray Bursts with Extended Emission Observed with BATSE

Zahide Funda Bostancı, Yuki Kaneko, Ersin Göğüş

Sabancı University, Faculty of Engineering and Natural Sciences, Orhanlı Tuzla 34956 Istanbul Turkey

ABSTRACT

We present the results of our systematic search for extended emission components following initial short gamma-ray burst (GRB) spikes, using Burst and Transient Source Experiment (BATSE) observations. We performed the extended emission search for both short- and long-duration GRBs to unveil the BATSE population of new hybrid class of GRBs similar to GRB 060614. For the identified bursts, we investigate temporal and spectral characteristics of their initial spikes as well as their extended emission. Our results reveal that the fraction of GRBs with extended emission is $\sim 7\%$ of the total number of our BATSE sample. We find that the spectrum of the extended emission is, in general, softer than that of the initial spike, which is in accord with what has been observed in the prototypical bursts, GRB 060614. We also find that the energy fluence of the extended emission varies on a broad range from 0.1 to 40 times of the fluence of the initial spike. We discuss our results in the context of existing physical models, in particular within the two-component jet model.

Key words: gamma ray bursts: general - method:search for extended emission

1 INTRODUCTION

Gamma ray bursts (GRBs) are traditionally divided into long and short classes, based on the bimodality in the duration distribution and spectral hardness (Kouveliotou et al. 1993) as observed with the Burst and Transient Source Experiment (BATSE). However, there is no clear dividing line for the two classes as their distributions significantly overlap. Another ambiguity arises from the fact that the observed GRB durations could be dilated due to cosmological redshifts ($\langle z \rangle \sim 2-3$, the most distant so far with $z \sim 9.4$; e.g., Jakobsson et al. 2012; Cucchiara et al. 2011), which vary from burst to burst. Long GRBs, with a duration greater than a few seconds, are generally distinguished by softer spectra and show spectral lag, which is the time difference of arrival photon in separate energy range, while short GRBs are characterized by harder spectra and have negligible spectral lags (Norris, Marani, & Bonnell 2000).

It is mostly believed that the physical origins of long and short bursts are different although the generation mechanism of GRBs is still uncertain. Afterglow observations show that long GRBs usually originate from star forming region in late type galaxies (Fruchter et al. 2006; Levesque et al. 2010), and some have accompanying supernovae likely caused by the core collapse of massive stars (collapsar; Woosley 1993). Short GRBs, on the other hand, could be the results of mergers of binary compact objects, such as two neutron stars or a neutron star and a black hole (Paczynski 1986; Eichler et al. 1989; Narayan et al. 1992).

Both early and late types of host galaxies have been identified for short GRBs and no supernova association with short GRBs has been observed although they seem to occur relatively nearby (see Berger 2011, for a review).

The classification of long and short GRBs is further complicated by the fact that some GRBs exhibit softer, low intensity Extended Emission (EE) components following the initial short-hard spikes. Duration of the first component is usually shorter than 5 s, whereas the second component occurs in time intervals from several seconds up to ~ 100 s, usually with gaps of 5 – 10 s between the spike and the EE component. The durations, T_{90} ¹, and subsequent classification of these GRBs then depend on the brightness and the hardness of the EE components. Such EE has been observed with various experiments (e.g., Barthelmy et al. 2005; Villasenor et al. 2005; Gehrels et al. 2006). Specifically, in the Konus catalog, the EE was found in 11 of short events (Mazets et al. 2002; Frederiks et al 2004); in the BATSE samples, it was visually identified in 8 bursts, all of which are traditionally classified as long GRBs (Norris & Bonnell 2006); and in the second *Swift* Burst Alert Telescope (BAT) catalog, 10 short GRBs with EE were identified (Sakamoto et al 2011; Norris, Gehrels, & Scargle 2010). In addition, long duration burst tails (or early afterglows) have been de-

¹ T_{90} is the time during which 90% of event photons were collected.

tected in the summed light curves of short GRBs in the BATSE data (Lazzati, Ramirez-Ruiz, & Ghisellini 2001; Connaughton 2002), in Konus (Frederiks et al 2004), and in BeppoSAX (Montanari et al. 2005). Note that these might refer to a different phenomenological aspect of short events, although such burst tails might result from the superposition of GRBs with weak EE. Since all these GRBs with EE seem morphologically and spectrally similar, it is possible that they have the same physical origin regardless of their classifications based solely on their T_{90} measurements. If so, they may comprise a new class of GRBs that possess some properties of both short-hard and long-soft GRBs.

A defining example of such a new class GRB is GRB 060614 (Gehrels et al. 2006). The burst was observed with *Swift* BAT and was a long event ($T_{90} = 102$ s) as determined with the BAT in the energy range of 15–350 keV. It contained a short hard spike with a duration less than 5 s and a soft EE with a duration of ~ 100 s, which was 5 times more energetic than the short spike. They found that, albeit the long duration, its temporal lag and peak luminosity fall within the short GRB subclass. In addition, no supernova association was detected from this event down to a very low limit (R-band magnitude $\gtrsim 23$), although it was originated in rather nearby star-forming galaxy at $z = 0.125$ (Fynbo et al. 2006; Gal-Yam et al. 2006; Della Valle et al. 2006). The original classification of the long and short GRBs was based on the BATSE GRB sample, which was sensitive to slightly higher energy ($\gtrsim 30$ keV) than BAT. In fact, based on the spectra, BATSE would have identified GRB 060614 with much shorter T_{90} due to the very soft nature of the EE component. Therefore, the combination of long and short GRB properties of this burst calls for the new class of GRBs, which may require a different progenitor scenario than the currently accepted physical models for long and short GRBs.

Such extended emission could be due to the prolonged activity of the central engine; however, the long timescale is difficult to reconcile with the merger model, while the non-association of a supernova in this case is not in agreement with the standard collapsar model. At least for the case of GRB 060614, the EE being an early X-ray afterglow is unlikely due to its similarity in spectral lag to the initial spike, as well as its high variability (Gehrels et al. 2006).

In this study, we performed a systematic search for GRBs that are similar to GRB 060614 using BATSE GRB data archive, to identify GRBs with EE that may constitute the possible new class. On board the *Compton Gamma Ray Observatory* (CGRO), BATSE recorded 2704 GRBs, of which $\sim 25\%$ are classified as “short” by the traditional definition of $T_{90} < 2$ s. In our search, we included all GRBs, both short and long. We present the results of our systematic search, and temporal and spectral properties of the identified bursts. We organize the paper as follows. In § 2 after a brief description of the BATSE instrument and data types, we explain the background determination and the search methodology of our study. In § 3 we give the search results and examine spectral properties of our findings. Finally, in § 4 we discuss the results in the context of related physical models.

2 DATA TYPES AND SEARCH METHOD

We first give a brief description of the BATSE instrument and of the data types that we used for our analysis (for a detailed description, see Fishman et al. 1989; Preece et al. 2000; Kaneko et al. 2006).

2.1 Data Types

BATSE consisted of eight identical detector modules located at the corners of the CGRO spacecraft for the whole-sky coverage. Each module had two NaI(Tl) scintillation detectors: a Large Area Detector (LAD; constant energy coverage of ~ 30 –2000 keV) and a Spectroscopy Detector (SD; variable energy coverage between ~ 5 keV and 20 MeV). The data were collected continuously in low-resolution non-burst mode, and high-resolution burst-mode data were accumulated when a burst was triggered. They were then processed in the data processing unit to construct various data types with different time and energy resolutions.

Although the SD provided a broader energy coverage, the LAD was more sensitive having a photon collecting area that was 16 times larger than the SDs. For our search, the data with higher sensitivity are desirable to identify possibly weak EE components. Therefore, we used the LAD data of the following types for this study: Discriminator data (DISCLA), Continuous data (CONT), Time-Tagged Event data (TTE), Discriminator Science data (DISCSC), and Medium Energy Resolution data (MER). DISCLA and CONT were continuous, non-burst mode data. The DISCLA data provided four energy channels (CH 1–4 corresponding to ~ 25 –50, 50–100, 100–300 and > 300 keV) with 1.024-s time resolution, while CONT data provided 16 energy channels with 2.048-s resolution. TTE, DISCSC and MER were burst mode data. The TTE and DISCSC data provided four energy channels (same as DISCLA) and TTE data were time tagged with a minimum of 2 ms resolution, while DISCSC data had 64-ms time resolution. Finally, the MER data provided 16 energy channels with 16 ms time resolution for the first 32.768 s and 64 ms up to 163.84 s after the trigger. We note that the DISCSC and MER data consist of summed data of 2–4 brightest detectors (i.e., detectors which recorded highest counts from the source), whereas all of the other data types are for individual detectors.

2.2 Background Determination and Search Criteria

For the systematic search for GRBs with EE, we used DISCLA data collected with the two brightest detectors for each GRB. We only considered lowest two channels of DISCLA (25–50 and 50–100 keV) since the EE component is usually softer than the initial spike component.

Determination of background rates plays a critical role in this study because correct identification of EE component can only be achieved with the subtraction of accurate background from the burst light curves. Since the orbit of CGRO was at the same geomagnetic coordinates every 15 orbital periods (~ 24 hours), the background rates at a burst trigger time T_0 could be approximated by averaging the rates at times $T_0 \pm 15$ orbits (Connaughton 2002). Therefore, we

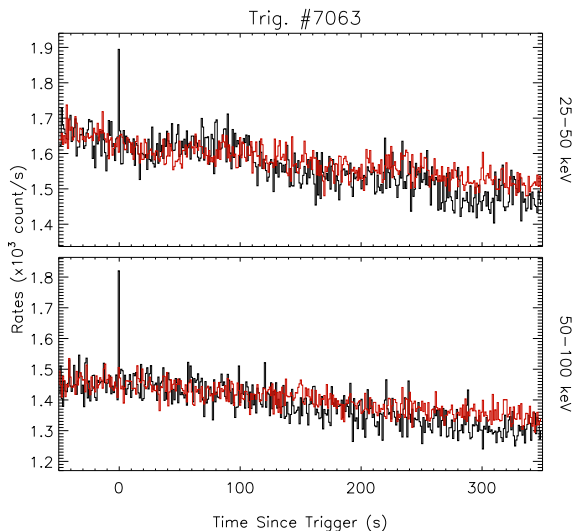


Figure 1. Light curves (black line) of GRB 980904 (BATSE Trigger 7063) in two energy bands and orbital backgrounds (red line) determined using $T_0 \pm 15$ orbits.

obtained a background measurement by using the average of the rates of the two orbits.

We first took into account short GRBs with duration $T_{90} \leq 5$ s. We found 648 such events from the duration table of the Current BATSE GRB Catalog², which contains 2041 bursts. We then subtracted the orbital background from the observed count rates in each of the two energy channels. In the case where we could not find the background rates at times $T_0 \pm 15$ orbits, we used the rates from $T_0 \pm 30$ orbits (2 days before and after), or $T_0 \pm 45$ orbits. Figure 1 shows an example of the orbital background. There were cases, however, in which no acceptable background was found either due to data gaps or obvious background mismatches with the data of $T_0 \pm 15$, 30, and 45 orbits. These bursts were thus excluded from our investigation.

2.3 Search Criteria

Based on earlier reports of such EE, we focused in the time interval between $T_0 + 5$ and $T_0 + 350$ s in search of EE. We binned the data of this time interval to 4-s resolution and calculated the Signal to Noise Ratio (SNR) of each bin. We positively identified EE when $\text{SNR} \geq 1.5\sigma$ above the background for at least consecutive 12 s in both detectors. Inclusion of the second brightest detector ensures that the EE component detection is not serendipitous.

Out of 648 short-duration GRBs ($T_{90} \leq 5$ s) in the BATSE catalog, valid orbital background lightcurves were found only for 269 GRBs. The orbital background data for the other 313 GRBs were unavailable, likely due to frequent spacecraft re-orientation. So we scanned these events with the above criteria for the EE search. There are, however, some long GRBs ($T_{90} > 5$ s) that also can be classified as a burst with a short spike and EE (e.g., Norris et al. 2006). This can occur when the EE components are bright enough

to contribute significantly to the total photon fluence of the event. To also identify such events in our search, we defined additional morphological criteria for the 1393 long GRBs ($T_{90} > 5$ s) in the BATSE catalog: the burst peak should occur before $T_0 + 5$ s, and the count rates should remain below 10% of the peak count rate for at least 60% of the duration after the peak time until $T_0 + 5$ s. These criteria were applied using 64-ms DISCSC light curves (in 25–300 keV). The DISCSC data were available for 1373 events out of the 1393 long GRBs, of which 36 matched the morphological criteria. We then studied their background data and found that only 18 of them had valid background data. Consequently, a total of 18 long-duration GRBs were subjected to the EE search.

Finally, we also considered 663 GRBs without the duration information available in the catalog. We applied the criteria for the long GRBs explained above for these events. The DISCSC data were available for 535 of these GRBs, and of these, we identified 84 GRBs that matched the morphological criteria; however, due to incomplete DISCLA data or invalid background, only 9 of them were ultimately subjected to the further EE investigation.

3 SEARCH RESULTS AND ANALYSIS

After the systematic search for EE components using 296 BATSE GRBs with complete data and valid background, we identified a total of 47 GRBs with potential EE components. We then visually inspected the energy-resolved light curves of each of these events. We found that some of these were false detections due to occultation-like steps in the background (i.e., another bright source being occulted by the Earth) or inaccurate estimation of the background, and therefore were discarded from our candidate sample. We also checked their individual burst reports to exclude GRBs with some known X-ray sources (e.g., Cygnus X-1) or particle events in the background. As a result, there were 24 remaining GRBs that consist of short spikes followed by EE. However, one of them (trig 5989) had EE with three defined peaks, which resembles a multi-episodic long GRB. Therefore, we removed it from our sample. We note that only two of the eight events previously identified by Norris & Bonnell (2006) were identified in our search. This is because the other six events did not meet our morphological criteria for long GRBs, or if they did, no valid orbital background data were available.

Some of the identified EE were very dim, barely above the 1.5σ cutoff. In order to perform statistically significant analysis on the identified EE components, we selected all events with a total $\text{SNR} \geq 20$ for the entire EE component in CH 1. It should be noted that there were a few cases in which the EE was detected only in CH 2, so the SNR criterion was applied to CH 2 in such cases.

After applying these criteria, we found 19 GRBs with statistically significant EE. In Figure 2, we present the example light curves of two GRBs with identified EE components³. Among these GRBs, 11 are short bursts by the traditional definition of $T_{90} < 2$ s and seven of them are long

² <http://gammaray.nsstc.nasa.gov/batse/grb/catalog/current/>

³ All 19 lightcurves are currently available at http://people.sabanciuniv.edu/fbostanci/GRB_EE/

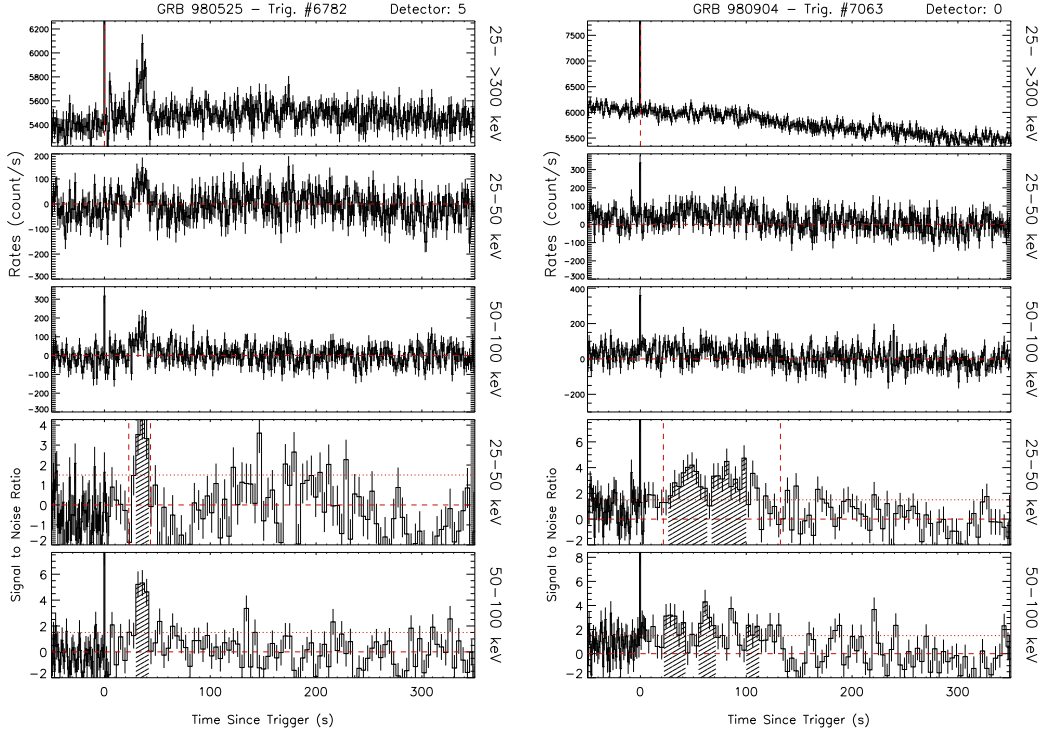


Figure 2. Example light curves of the brightest detectors of two GRBs with EE. For both GRBs, top panel shows sum of four energy channels, the second and third panels are background subtracted light curves in two lowest energy channels. The horizontal red dashed line indicates the level of the background. The last two panels show signal to noise ratio as a function of time. The shaded areas indicate the time ranges where the SNR is $\geq 1.5\sigma$ for at least consecutive 12 s, and the horizontal dashed and dotted lines show the background level and the 1.5σ level, respectively. The vertical red dashed lines indicate time interval of EE component, which was subjected to the spectral analysis.

events ($T_{90} > 2$ s). The durations of the spikes and the EE range in 0.18–4.86 s and 12–133 s, respectively (see Table 1). One of them (GRB 990712, trig 7647) does not have duration information. We estimated the duration of this GRB as $T_{90} = 67.8 \pm 2.1$ s using cumulative photon fluence, indicating that it belongs to the long. In case more than one segment of the excess emission were found, we determined the duration of the detected EE components by assuming that the EE was continuous from the first segment to the last, based on the lowest energy light curve (25–50 keV).

3.1 Spectral Lag Analysis

In our exploration of the general properties of these GRBs, we first investigated the spectral lags of their initial spikes. We used the four-channel TTE data binned to 8-ms resolution in the time range from $T_0 - 0.2$ to $T_0 + 5$ s, and computed the spectral lag of the signals in CH1 with CH3 by using a cross correlation function (see e.g., Norris, Marani, & Bonnell 2000). For GRBs 970918 and 980525 the spikes were not significant enough in CH1; therefore, for these bursts we used CH2 and CH3 for the lag calculations. We estimated the uncertainties in the lag measurements through simulations as follows: For each of these bursts, we generated simulated light curves in CH1 and CH3 using a two sided Gaussian function whose left-width is set by the rise time of the initial spike, the right-width is set by the decay time, and the amplitude is set to the max-

imum rate in the particular energy band. The peak time of the simulated CH3 curve is shifted by the measured lag value of the burst. Using the same cross calibration method, we calculated the lag between the two channels. For each burst, we iterated this procedure 100 times and calculated the root-mean-square value of the difference between the lag calculated with the simulated light curves with respect to the measured value, which was used as the uncertainty in the time lag.

For most of the bursts the spectral lags of the spikes were less than 10 ms (see Table 1). Although no redshift values are known for any of these GRBs, the lag values are consistent with those found for nearby short GRBs (Gehrels et al. 2006), if we assume typical redshift values for short GRBs of $z \lesssim 1$ (Berger 2011) for these events. We note that although our sample size is small, there is no significant correlation between the peak flux and the spectral lags for the spikes (see Figure 3), consistent with the properties of short GRBs (Norris, Marani, & Bonnell 2000). The spectral lags for the spikes of most of these events are also found in the BATSE spectral lag database (Hakkila et al. 2007). There, they used 64-ms DISCSC data to calculate the lags, while we used 8-ms TTE data to obtain our results. The values are nonetheless mostly consistent within uncertainties.

For the EE components, we were only able to calculate the lags for four events with pronounced peaks in the EE light curves; those are Trigger numbers 1997, 2436, 6782, and

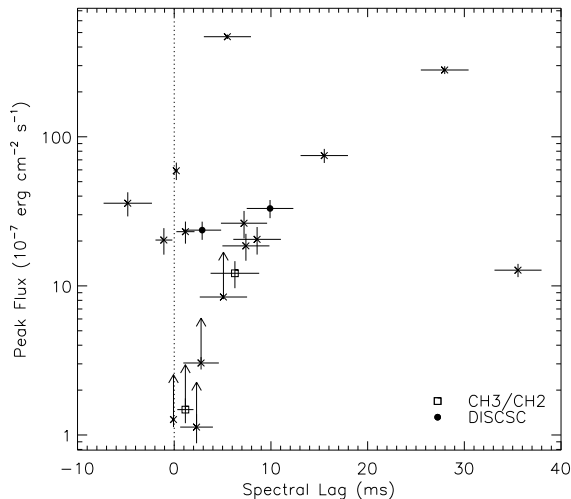


Figure 3. Spectral lag vs. peak flux. The lags are between CH 1 and CH 3 of TTE data, and peak flux is in 30–1500 keV (from Table 2). The arrows show CONT events’ peak flux, which should be taken as the lower limits. Squares show two events with lags calculated using CH 2 and CH 3. Filled circles show events for which DISCSC data were used for the lags. No significant correlation was found (correlation coefficient, $R = 0.29$, chance probability $P = 0.24$.)

Table 1. Durations of the spikes and the extended emission, T_{90} from the BATSE GRB Catalog, and spectral lags of the spikes for the 19 GRBs with EE. T_{Spike} and T_{EE} were estimated using 64-ms resolution data.

Trig#	GRB name	T_{Spike} (s)	T_{EE} (s)	T_{90} (s)	Spectral Lag (ms)
0575	910725	0.53	85.60	0.41	7.41 ± 2.43
0603	910802	1.22	133.3	1.47	2.89 ± 1.96
0906	911016	0.53	112.2	0.40	7.22 ± 2.39
1088	911119	0.18	81.39	0.19	9.91 ± 2.41
1719	920722	0.59	12.14	1.05	8.57 ± 2.46
1997	921022	1.04	116.7	60.22	5.09 ± 2.45
2436	930709	4.86	29.20	33.28	0.22 ± 0.16
2611	931931	3.71	12.01	12.21	27.97 ± 2.47
3611	950531	2.75	55.29	3.52	-0.08 ± 0.06
3940	951211	0.67	38.46	0.58	-1.07 ± 0.87
5592	960906	0.45	87.04	0.48	1.16 ± 0.94
5634	961017	1.42	45.33	1.15	35.55 ± 2.43
6385	970918	0.29	14.66	0.90	6.27 ± 2.51
6569	980112	1.22	81.89	0.94	2.31 ± 1.69
6782	980525	1.37	22.53	39.68	1.15 ± 0.84
7063	980904	0.45	110.6	0.13	2.78 ± 1.84
7446	990304	3.45	16.27	13.57	15.52 ± 2.45
7599	990605	1.00	24.19	6.34	-4.80 ± 2.50
7647	990712	0.75	78.85	67.8	5.50 ± 2.44

7647. The lag values are 15.8 ± 21.1 , 48.1 ± 21.0 , 87.7 ± 19.7 , and -22.0 ± 21.2 ms, respectively. Two of them show no lags, while for the other two the lags are marginally larger than those of the spikes. These lags are comparable to the average lag of long GRBs (~ 50 ms; Norris, Marani, & Bonnell 2000).

3.2 Spectral Analysis

We also analyzed the spectra of the initial spikes and the EE components of these GRBs. We used MER data (or CONT data in case there is no MER data). Since the lowest one or two channels of the MER/CONT data are usually below the electronic threshold, and the highest channel is an energy overflow channel, we used a total of about 14 energy channels (~ 30 –1800 keV) for each spectral analysis.

We performed the spectral fitting with the RMFIT¹ version 4.0rc1. For each event, we analyzed the spectra of the initial spike and of the EE separately. The durations of the EE used for the analysis were matched to the time intervals where the excess emission was identified by the search algorithm. We employed three photon models: a single power-law model (PWRL), Comptonized (power law with exponential cutoff) model with E_{peak} parametrization² (COMP), and the empirical GRB function (BAND; Band et al. 1993). We determined the simplest, statistically well-fit model for the spectra of the spike and the EE. We also took into account the spectral parameter constraints. We present the spectral analysis results with the best model for each component in Table 2.

We find that either PWRL or COMP was sufficient to describe all of the spikes as well as the EE components, with most of the spikes (EE) are best fit with the COMP (PWRL) model. Based on the hardness ratios (calculated with the photon flux of the best fit model, see Table 2), the spectra of the EE components are usually softer, in accord with previous works in literature. In only one case (Trigger number 5634), the EE component is harder than the spike. We note that the resulting χ^2 of the spike spectrum fit of this event is rather large (22.4 for 11 degrees of freedom, dof). This is due to some low-energy feature in the data, which likely comes from the spectral evolution within the spike. Although we do not present time-resolved spectral analysis here, some of these 19 events show significant spectral evolution in both the spikes and EE (see also Kaneko et al. 2006), which result in such large χ^2 values in time-integrated spectral modeling. In particular, the spectral data of trigger number 5634 could statistically be better described with models containing multi-spectral components, such as black-body plus COMP. This, however, does not affect the total fluence values significantly and hence does not change the hardness ratio estimate.

We find a significant anti-correlation between the duration and the hardness ratio of both spikes and EE combined (correlation coefficient, $R = -0.63$, and chance probability, $P = 2.55 \times 10^{-5}$). The spike spectra are on the hard side in terms of E_{peak} values compared to the mean value of ~ 320 keV derived from time-integrated spectra of bright BATSE GRBs (Kaneko et al. 2006). The mean value of the PWRL indices for EE is -2.21 ± 0.30 . The fact that larger fraction of the EE components are better fit with PWRL could be due to either the real intrinsic soft nature or the low statistics. The energy fluence ratios of the EE to spike,

¹ R. S. Mallozzi, R. D. Preece, & M. S. Briggs, "RMFIT, A Lightcurve and Spectral Analysis Tool," © Robert D. Preece, University of Alabama in Huntsville.

² $f(E) = A \exp[-E(2 + \lambda)/E_{\text{peak}}](E/E_{\text{piv}})^{\lambda}$

in the 30–1500 keV range vary from ~ 0.1 to ~ 40 but most of them have values around one to a few (see Table 2).

We note that in some cases, EE spectra did not provide well-constrained parameters or could not be fitted at all due to low statistics. The EE of these GRBs were identified only in one energy channel (mostly CH 1 but one GRB in CH 2), and even though the SNR in the identified energy channel is sufficiently high, their broadband spectra did not afford adequate total SNR for the parameter constraints. Nevertheless, these spectra provide reliable estimates on their relative hardness and energy fluence. It should also be noted that the EE spectrum of another event (Trigger 603) is fit with COMP with $E_{\text{peak}} = 1126$ keV and $\lambda < -2$, indicating that the model describes a power law with exponential *increase* above the E_{peak} . This is due to excess emission at higher energies.

4 DISCUSSION

Based on a systematic search of 296 GRBs from the BATSE archive, we identified 19 GRBs with EE that comply with our criteria with sufficient statistics. 11 of these events are classified as short and 8 were long GRBs, based on the traditional dividing line of $T_{90} = 2$ s. The fraction of the BATSE GRBs with EE is $\sim 7\%$ of the total number of bursts consisting of initial short spikes, and having valid background data. It has previously been reported that the fraction of the *Swift* BAT short GRBs with EE corresponds to 2% of the second BAT catalog (Sakamoto et al 2011), and 25% of BAT short GRBs (Norris, Gehrels, & Scargle 2010). We caution that these statistics are not directly comparable since the criteria and methods used for the searches as well as for the parent sample selection were different. Nevertheless, some discrepancy in the EE detection frequencies is expected due to the differences in the instrumental responses and triggering algorithms of BATSE and BAT. BAT triggers on smaller fraction of short GRBs ($\sim 10\%$ of all BAT GRBs) compared to the BATSE sample but more sensitive to the softer EE components once they are triggered. Moreover, our statistics regarding the fraction of short GRBs with EE should be taken only as a lower limit. This is because the detection of EE components depends on the detection threshold of the observing instruments as pointed out by Norris, Gehrels, & Scargle (2010), since most of the EE components are very weak. Especially considering relatively lower sensitivity of BATSE LAD in energies $\lesssim 100$ keV and the soft nature of the EE, as well as relatively noisy background in BATSE data, possibly a larger fraction of the BATSE short GRBs are accompanied by EE. We note, however, Norris, Gehrels, & Scargle (2010) estimates that such EE would have been detected in as much as 50% of *Swift* BAT short GRBs if it had been present, after taking into account the the detector sensitivity, suggesting that there is a physical threshold for the EE and only $\sim 25\%$ of short GRBs are really associated with EE.

The spectral lags of the spikes of the 19 GRBs are small with most of them $\lesssim 10$ ms, consistent with other short-duration GRBs. For the EE, we were able to determine the lags for four events, two of which indicate no spectral lags and the other two comparable to those of long GRBs. In the case of GRB 060614, the spectral lag for the EE was

found to be insignificant similar to the spike, which may be suggestive of the same physical origin for both of the components. In contrast, our results may point to different origins for at least some of the EE, possibly caused by milder outflow with smaller Lorentz factor than the origin of the spikes.

The spike and EE components are both well described with either a single power law model or a Comptonized model. In all cases except one, the EE components are softer than the spike based on their hardness ratios. The energy fluence ratio of the two components ($E_{\text{EE}}/E_{\text{spike}}$) spans a wide range, varying from ~ 0.1 to ~ 40 , as was also found by Norris & Bonnell (2006), who also searched visually GRBs with EE within the BATSE archive and identified eight GRBs with EE. Among the eight events of Norris & Bonnell (2006), only two were identified in our systematic search (Triggers 1997 and 7647). They reported that EE component is always softer than the initial spike as determined by their hardness ratios. Our results confirm the soft nature of the EE in general, although several GRBs in our sample have EE that are comparably as hard as, or harder than the corresponding spikes.

Based on the spectral analysis, at least four events (Trigger numbers 1088, 1997, 6385, and 6569) are spectrally very similar to GRB 060614. The spectral lags of the spikes of all these events are of the order of a millisecond, also similar to 060614 although our uncertainties are smaller. All of them consist of a spike $\lesssim 1.5$ s, and the EE of three of them are ~ 100 s while the other has a short EE of about 15 s. The peak (isotropic) luminosity of 060614 spike was $1.5 \times 10^{50} \text{ erg s}^{-1}$. If we assume the same cosmological redshift as 060614 ($z = 0.125$), the peak luminosity estimates for these four events are in the range of $4.5 \times 10^{48} - 4 \times 10^{50} \text{ erg s}^{-1}$.

The nature of the EE may be explained by the interaction of relativistic outflow with the circumburst medium (i.e. early afterglow) or late time central engine activity. However, the temporal variations in the light curves of some bright EE increase the possibility of ongoing central engine activity.

The collapsar model for long bursts could produce a burst consisting of a short-hard spike and EE in various scenarios. Zhang, Woosley, & MacFadyen (2003) showed that the short-hard “precursor” is created due to the relativistic jet breakout and subsequent interaction with the surrounding stellar wind. The following long, main burst component is then created by the internal shocks. The relative brightness of the short precursor and the main burst component can vary greatly, as it depends on many physical parameters at two different origins. Another model was proposed by Lazzati, Morsony & Begelman (2010), in which the EE in short GRBs could be created in collapsar viewed off axis. A critical piece of observational evidence for these model is a supernova association, which extensive follow-up optical observations have excluded for some short GRBs with EE (Hjorth et al. 2005; Gal-Yam et al. 2006; Fynbo et al. 2006; Perley et al. 2009). These models also expect that the bursts take place in active star-forming regions of the host galaxies, which have also been ruled out for many short GRBs whose host galaxies have been identified (Gehrels et al. 2005; Villaseñor et al. 2005; Barthelmy et al. 2005). Unfortunately, there was no follow-up observations in

Table 2. Summary of spectral fit results of 19 GRBs with EE.

Trig#	GRB Date	Data Type	Component	Time interval (s)	Model	A ^a	E _{peak} (keV)	λ	χ ² /dof	Energy ^b Fluence	F _{peak} ^c	HR _{3/2} ^d
0575	910725	MER	Spike	0.02 : 0.55	COMP	10.0 ± 1.2	413 ± 81	-0.82 ± 0.17	19.5/11	1.76 ± 0.07	18.6 ± 3.8	1.50 ± 0.12
			EE	4.41 : 90.01	PWRL	0.20 ± 0.04	-	-2.57 ± 0.26	15.2/12	11.25 ± 1.37	0.60 ± 0.22	0.46 ± 0.15
0603	910802	MER	Spike	0.03 : 1.25	COMP	7.3 ± 1.1	340 ± 99	-1.26 ± 0.18	11.1/11	3.07 ± 0.11	23.7 ± 3.3	1.02 ± 0.07
			EE	5.68 : 139.04	COMP	0.27 ± 0.03	1126 ± 240	-2.57 ± 0.18	11.4/11	25.42 ± 2.53	6.8 ± 2.2	0.45 ± 0.09
0906	911016	MER	Spike	0.02 : 0.55	COMP	12.7 ± 1.4	420 ± 55	-0.37 ± 0.18	14.2/11	2.20 ± 0.07	26.3 ± 5.5	1.86 ± 0.16
			EE	5.10 : 117.27	PWRL	0.16 ± 0.04	-	-1.42 ± 0.23	8.2/12	8.45 ± 1.91	5.9 ± 2.2	1.11 ± 0.40
1088	911119	MER	Spike	0.03 : 0.20	COMP	17.3 ± 4.3	282 ± 48	-0.37 ± 0.34	9.9/11	0.72 ± 0.04	33.1 ± 4.6	1.61 ± 0.19
			EE	10.28 : 91.67	PWRL	0.25 ± 0.03	-	-2.06 ± 0.19	5.7/12	10.07 ± 1.30	6.6 ± 1.9	0.69 ± 0.14
1719	920722	MER	Spike	0.02 : 0.62	COMP	8.5 ± 0.7	548 ± 63	-0.14 ± 0.18	14.4/9	2.05 ± 0.07	20.5 ± 4.3	2.55 ± 0.26
			EE*	46.66 : 58.80	-	-	-	-	-	-	-	-
1997	921022	CONT	Spike	-2.75 : 3.39	PWRL	3.9 ± 0.1	-	-1.76 ± 0.04	10.2/11	10.93 ± 0.27	102 ± 5	0.85 ± 0.03
			EE	3.39 : 120.13	PWRL	3.51 ± 0.04	-	-2.09 ± 0.02	13.2/11	204.40 ± 2.22	20.4 ± 2.6	0.64 ± 0.01
2436	930709	MER	Spike	0.03 : 4.90	COMP	15.9 ± 0.5	418 ± 16	-0.54 ± 0.05	20.6/11	25.24 ± 0.24	59.2 ± 7.9	1.58 ± 0.03
			EE	8.85 : 38.05	COMP	70.8 ± 0.2	354 ± 20	-1.20 ± 0.04	15.5/11	70.59 ± 0.56	17.0 ± 4.6	1.01 ± 0.02
2611	931031	MER	Spike	0.03 : 3.74	COMP	42.9 ± 0.5	658 ± 24	-1.18 ± 0.02	65.2/10	62.80 ± 0.33	280 ± 17	1.30 ± 0.01
			EE	5.82 : 17.83	PWRL	1.58 ± 0.06	-	-2.16 ± 0.06	16.4/11	9.76 ± 0.31	6.8 ± 2.1	0.65 ± 0.04
3611	950531	CONT	Spike	-3.07 : 7.17	PWRL	0.4 ± 0.1	-	-3.20 ± 0.26	14.1/12	5.70 ± 0.79	1.27 ± 0.14	0.23 ± 0.08
			EE	19.46 : 74.75	PWRL	0.2 ± 0.1	-	-2.77 ± 0.65	4.4/12	7.01 ± 2.38	0.34 ± 0.12	0.34 ± 0.27
3940	951211	MER	Spike	0.03 : 0.70	COMP	16.5 ± 2.6	231 ± 24	-0.73 ± 0.18	15.9/11	2.50 ± 0.07	20.3 ± 4.1	1.22 ± 0.07
			EE	4.89 : 43.35	PWRL	0.19 ± 0.04	-	-2.65 ± 0.28	15.9/12	5.07 ± 0.73	2.3 ± 1.6	0.43 ± 0.14
5592	960906	MER	Spike	0.02 : 0.47	PWRL	3.8 ± 0.3	-	-1.48 ± 0.11	7.0/12	0.76 ± 0.07	23.1 ± 3.9	1.01 ± 0.14
			EE	10.01 : 97.05	PWRL	0.19 ± 0.04	-	-1.64 ± 0.27	17.2/11	7.58 ± 1.39	3.8 ± 2.0	0.88 ± 0.27
5634	961017	MER	Spike	0.03 : 1.45	COMP	57 ± 12	57 ± 3	-1.10 ± 0.15	22.4/11	6.87 ± 0.21	12.8 ± 1.3	0.40 ± 0.02
			EE	5.04 : 50.33	PWRL	0.07 ± 0.03	-	-1.19 ± 0.31	11.3/10	1.62 ± 0.63	10.0 ± 2.8	1.42 ± 0.86
6385	970918	MER	Spike	0.02 : 0.31	COMP	29.3 ± 7.1	265 ± 24	0.81 ± 0.38	15.5/10	1.41 ± 0.06	12.2 ± 2.5	2.46 ± 0.28
			EE	22.34 : 37.02	PWRL	0.13 ± 0.05	-	-1.99 ± 0.68	14.7/11	0.92 ± 0.37	5.3 ± 2.6	0.66 ± 0.46
6569	980112	CONT	Spike	-1.66 : 4.48	PWRL	0.7 ± 0.1	-	-1.81 ± 0.22	13.0/12	1.94 ± 0.27	1.13 ± 0.25	0.81 ± 0.19
			EE	18.82 : 100.74	PWRL	0.33 ± 0.07	-	-1.99 ± 0.34	15.4/12	12.84 ± 2.70	0.41 ± 0.15	0.70 ± 0.26
6782	980525	CONT	Spike	-3.58 : 2.56	PWRL	0.4 ± 0.1	-	-1.34 ± 0.25	8.2/12	1.12 ± 0.25	1.48 ± 0.28	1.26 ± 0.45
			EE	20.99 : 43.52	PWRL	0.50 ± 0.05	-	-1.68 ± 0.16	15.0/12	5.08 ± 0.54	0.99 ± 0.25	0.94 ± 0.16
7063	980904	CONT	Spike	-2.88 : 3.26	PWRL	0.7 ± 0.1	-	-1.19 ± 0.12	14.4/12	2.09 ± 0.27	3.04 ± 0.29	1.35 ± 0.29
			EE	21.70 : 132.29	PWRL	0.13 ± 0.07	-	-2.59 ± 0.67	6.8/12	8.96 ± 2.76	0.78 ± 0.27	0.41 ± 0.34
7446	990304	MER	Spike	0.02 : 3.48	COMP	30.8 ± 1.1	224 ± 12	-1.44 ± 0.03	14.6/10	34.49 ± 0.24	74.8 ± 8.1	0.82 ± 0.01
			EE	5.99 : 22.26	PWRL	0.71 ± 0.05	-	-2.29 ± 0.11	10.3/11	6.11 ± 0.36	2.5 ± 1.6	0.51 ± 0.06
7599	990605	MER	Spike	0.03 : 1.04	COMP	5.3 ± 0.5	593 ± 91	-0.15 ± 0.22	4.5/10	2.25 ± 0.10	35.8 ± 6.6	2.51 ± 0.31
			EE	14.30 : 38.49	PWRL	0.02 ± 0.04	-	-4.33 ± $1.23_{1.72}$	13.7/11	2.14 ± 2.37	7.9 ± 2.3	0.12 ± 0.32
7647	990712	MER	Spike	0.02 : 0.78	COMP	73.1 ± 0.7	1230 ± 29	-0.40 ± 0.02	25.7/10	29.02 ± 0.19	469 ± 16	2.25 ± 0.03
			EE	4.50 : 83.35	PWRL	1.4 ± 0.1	-	-1.96 ± 0.13	8.6/10	52.13 ± 4.49	8.1 ± 2.0	0.66 ± 0.09

All uncertainties are 1σ .

^a in units of 10^{-3} photons $\text{cm}^{-2} \text{s}^{-2} \text{keV}^{-1}$

^b in units of 10^{-7} erg cm^{-2} and calculated in the 15–350 keV range

^c in units of 10^{-7} erg $\text{cm}^{-2} \text{s}^{-1}$ and calculated in the 30–1500 keV range with 64-ms (MER) or 2-s (CONT) resolution

^d calculated in the 50 – 100 keV and 100 – 300 keV ranges

* too dim to perform the spectral fit.

longer wavelengths for the GRBs with EE in our sample to search for such associations.

Alternatively, MacFadyen, Ramirez-Ruiz, & Zhang (2005) have proposed that accretion-induced collapse of a neutron star into a black hole, similar to Type Ia supernova, may also be able to produce EE, if the jet from the accretion interacts with the envelope of a companion giant star. In this case, a supernova may not be created and the host galaxies can be both early and late types due to the widely-varying timescale in which the sequence of the events occurs. The high variability observed in some of the EE, however, may be difficult to reconcile with this model.

On the other hand, short GRBs with EE could also be produced in the context of the merger model of short GRBs, since the central engine may produce a relativistic outflow made of two different components. Metzger, Quataert, & Thompson (2008) and Bucciantini et al. (2012) have shown that these GRBs could be created by a protomagnetar (highly-magnetized, rapidly-rotating neutron star), formed either in accretion-induced collapse of a white dwarf, or in a merger of white dwarf bi-

nary or neutron star binary. In this scenario, the initial spike of the GRB is produced by the accretion powered jet, while the EE originates from a jet powered by the spin down of the protomagnetar, as it breaks out of the confined envelope of ejected mass. The large variation in the observed energy ratio of the spike and EE may also be explained by a possible wide range in initial angular momentum of the system. Although no bright supernova would accompany such a collapse or merger process, a smaller scale supernova would be expected around 1 day after the burst. A peak in optical wavelength similar to this signature has been observed in at least one short GRB with bright EE (GRB 080503), albeit its inconclusive nature (Perley et al. 2009).

Recently, Barkov & Pozanenko (2011) suggested a two component jet model in the context of compact binary merger to explain short GRBs with EE. In this model, the short spike is due to a jet powered by neutrino heating ($\nu\bar{\nu}$ annihilation) while the EE results from a jet produced by the Blandford-Znajek (BZ) mechanism. The opening angle of the neutrino-powered jet ($\theta_{\nu\bar{\nu}}$) is typically of the order of ~ 0.1 (for Lorentz factor, $\Gamma > 100$; Aloy, Janka & Müller

Table 3. Estimated ratios of opening angles of the two jet components.

Trig#	GRB name	$E_{\text{EE}}/E_{\text{Spike}}$ (15–350 keV)	$\theta_{\text{BZ}}/\theta_{\nu\bar{\nu}}$
0575	910725	6.38	0.29
0603	910802	8.29	0.21
0906	911016	3.84	0.43
1088	911119	13.98	0.33
1997	921022	18.70	0.06
2436	930709	2.80	0.08
2611	931931	0.16	0.26
3611	950531	1.23	0.12
3940	951211	2.03	0.31
5592	960906	9.92	0.26
5634	961017	0.24	0.67
6385	970918	0.66	0.51
6569	980112	6.64	0.08
6782	980525	4.53	0.05
7063	980904	4.29	0.12
7446	990304	0.18	0.30
7599	990605	0.95	0.29
7647	990712	1.95	0.44

2005), which can be much larger than the BZ-powered jet, $\theta_{\text{BZ}} \sim 1/\Gamma$. Then, the wide range of the energetic ratios of the short spikes and EE can be explained by various off-axis viewing positions.

Barkov & Pozanenko (2011) also estimated the ratio of the opening angles ($\theta_{\text{BZ}}/\theta_{\nu\bar{\nu}}$) using the observed fluence of the spike and EE in the case of GRB 060614, based on the relation:

$$\frac{L_{\text{BZ}}}{L_{\nu\bar{\nu}}} \left(\frac{\theta_{\nu\bar{\nu}}}{\theta_{\text{BZ}}} \right)^2 \frac{t_{\text{BZ}}}{t_{\nu\bar{\nu}}} = \frac{E_{\text{EE}}}{E_{\text{spike}}} \quad (1)$$

Here, E_{EE} and E_{spike} are the observed energy fluence, and $t_{\nu\bar{\nu}}$ and t_{BZ} are durations of the spike and the EE, respectively. They estimate the luminosities of the both jets to be $L_{\text{BZ}} \approx 10^{48} \text{ erg s}^{-1}$ and $L_{\nu\bar{\nu}} \approx 3 \times 10^{50} \text{ erg s}^{-1}$, assuming typical physical parameters of the progenitor, such as the black hole mass, spin parameter, accretion rate, and disc viscosity. For GRB 060614, $\theta_{\text{BZ}}/\theta_{\nu\bar{\nu}} \sim 0.1$. Using this equation, we estimated the ratios of jet opening angles of our 18 GRBs with EE (see Table 3). Trigger number 1719 was excluded here because the energy fluence value for the EE was not obtainable due to its low statistics. The fluence values used for these estimates were calculated in the energy range of 15–350 keV, so as to allow direct comparison with the values obtained for GRB 060614. We find that the angle ratios, $\theta_{\text{BZ}}/\theta_{\nu\bar{\nu}}$, span a wide range from 0.05 to 0.67. The ratio is always less than one, meaning that the BZ jet (responsible for EE) is more narrowly collimated than the neutrino jet (spike). This also implies that (from the above equation) the ratio of average flux values are always less than the ratio of the luminosity estimates of the two components; namely, $\bar{F}_{\text{EE}}/\bar{F}_{\text{spike}} < L_{\text{BZ}}/L_{\nu\bar{\nu}}$. In turn, this indicates either $L_{\text{BZ}} < 10^{48} \text{ erg s}^{-1}$ or $L_{\nu\bar{\nu}} > 3 \times 10^{50} \text{ erg s}^{-1}$.

Interestingly, both GRBs for which significant spectral lags in the EE were found, have rather small angle ratios, $\theta_{\text{BZ}}/\theta_{\nu\bar{\nu}} < 0.1$. This may indicate much wider neutrino-powered jets and hence the smaller Γ for these events. Moreover, although we see no significant correlation between the

angle ratios and the spectral lags of the spikes, the event with the largest spike lag (Trigger 5634; $35.55 \pm 2.43 \text{ ms}$) has the largest angle ratio estimate. These are puzzling, however, since larger lags are expected from less collimated jet structures, if the spectral lags are solely due to the curvature effect. By comparison, the angle ratio estimated for GRB 060614 was also ~ 0.1 but no spectral lag for neither the spike nor the EE was found. Also, one of our sample with no spectral lag in the EE (Trigger 1997) has a small angle ratio of 0.06. In these cases, the collimation angle for the neutrino jet may still need to be sufficiently small, which in turn indicates much higher Γ for the BZ jet.

Finally, we note that some short GRBs with EE are observed to have X-ray flare-like re-brightening in their afterglow light curves (Barthelmy et al. 2005; Margutti et al. 2011). The X-ray flares are observed in lower energy ($\lesssim 10 \text{ keV}$), usually at around a few hundreds to thousands of seconds after the gamma-ray prompt emission. They can be very bright with relatively sharp rise and fall, and are normally superimposed on a smoothly decaying light curve (Chincarini et al. 2010). Their temporal and spectral properties as well as energetics are very similar to GRB prompt emission (at least for long GRBs), suggesting an internal origin related to the central engine activity. If the EE identified in our search extends down to a few keV, they could resemble X-ray flares occurring at a very early stage of the afterglow (e.g., La Parola et al. 2006).

ACKNOWLEDGMENTS

We thank the referee for valuable comments and suggestions. This project is funded by the Scientific and Technological Council of Turkey (TÜBİTAK grant number 109T755).

REFERENCES

- Aloy, M. A., Janka, H.-T. & Müller, E., 2003, *A&A*, 436, 273
- Band, D. L., et al., 1993, *ApJ*, 413, 281
- Barkov, M. V. & Pozanenko, A. S., 2011, *MNRAS*, 417, 2161
- Bartelmy, S. D., et al., 2005, *Nature* 438, 994
- Berger, E., 2011, *New Astronomy Reviews*, 55, 1
- Bucciantini, N., et al., 2012, *MNRAS*, 419, 1537
- Chincarini, G., et al., 2010, *MNRAS*, 406, 2113
- Connaughton, V., 2002 *ApJ* 567, 1028.
- Cucchiara, A., et al., 2011, *ApJ*, 736, 7
- Della Valle, M., et al., 2006, *Nature*, 444, 1050
- Eichler, D., Livio, M., Piran, T., Schramm, D. N., 1989, *Nature*, 340, 126
- Fishman, G.J., et al. 1989, in *Proc. Gamma Ray Observatory Science Workshop*, ed. W. N. Johnson (Greenbelt: NASA/GSFC), 39
- Frederiks, D. D., et al., 2004, *ASPC*, 312, 197
- Fruchter, A., et al., 2006, *Nature*, 441, 463.
- Fynbo, J. P. U., et al., 2006, *Nature*, 444, 1047
- Gal-Yam, A., et al., 2006, *Nature*, 444, 1053
- Gehrels, N., et al., 2005, *Nature*, 437, 851
- Gehrels, N., et al., 2006, *Nature*, 444, 1044
- Hakkila, J., et al., 2007, *ApJS*, 169, 62

- Hjorth, J., et al., 2005, *Nature*, 437, 859
 Jakobsson, P., et al., 2012, *ApJ*, 752, 62
 Kaneko, Y., et al., 2006, *ApJ*, 166, 298
 Kouveliotou, C., et al., 1993, *ApJ*, 413, 101
 La Parola, V., et al., 2006, *A&A*, 454, 753
 Lazzati, D., Ramirez-Ruiz, E., Ghisellini, G. 2001, *A&A*, 379L, 39
 Lazzati, D., Morsony, B.J., & Begelman, M.C. 2010, *ApJ*, 717, 239
 Lazzati, D., Ramirez-Ruiz, E., & Ghisellini, G., 2001, *A&A*, 379, L39
 Levesque, E. M., Kewley, L. J., Berger, E., Zahid, H. J., 2010, *AJ*, 140, 1557
 MacFadyen, A. I., Ramirez-Ruiz, E., & Zhang, W. 2005, arXiv:astro-ph/0510192v1
 Mazets, E. P. et al., 2002, *astro.ph*, 9219
 Margutti, R., et al. 2011, *MNRAS*, 417, 2144
 Metzger, B. D., Quataert, E., & Thompson, T. A. 2008, 385, 1455
 Montanari, E., Frontera, F., Guidorzi, C., Rapisarda, M., 2005, *ApJ*, 625L, 17
 Narayan, R., Paczynski, B., Piran, T., 1992, *ApJ*, 395L, 83
 Norris, J. P. & Bonnell, J. T., 2006, *ApJ*, 643, 266
 Norris, J.P., Gehrels, N., & Scargle, J.D., 2010, *ApJ*, 717, 411
 Norris, J. P., Marani, G. F., & Bonnell, J. T., 2000, *ApJ*, 534, 248
 Paczynski, B., 1986, *ApJ*, 308L, 43
 Perley, D. A., et al., 2005, *ApJ* 696, 1871
 Preece, R. D., et al. 2000, *ApJ*, 126, 19
 Sakamoto, T. et al., 2011, *ApJS*, 195, 2
 Villasenor, J. S., et al., 2005, *Nature*, 437, 855
 Woosley, S. E., 1993, *ApJ*, 405, 273.
 Zhang, W., Woosley, S. E., & MacFadyen, A. I., 2003, *ApJ*, 586, 356.